Synthesis and Characterization of ZnO-Fe_2O_3 Anode Material for Lithium-Ion Battery

A Dissertation submitted towards the partial fulfillment of
the requirement for the award of degree of

Master of Technology

In

Nano Science and Technology

Submitted By

Garima Sharma
2K11/NST/05

Under the supervision of

Dr. Amrish K. Panwar
(Assistant Professor)

Department of Applied Physics

Delhi Technological University

(Formerly Delhi College of Engineering)

CERTIFICATE

This is to certify that the dissertation title ***"Synthesis and Characterization of ZnO-Fe_2O_3 Anode Material for Lithium-Ion Battery"*** is the authentic work of **Garima Sharma** under my guidance and supervision in the partial fulfillment of requirement towards the degree of Master of Technology in ***Nano Science and Technology*** run by the Department of Applied Physics in ***Delhi Technological University.***

Dr. Amrish K. Panwar
Supervisor, Assistant Professor
Department of Applied Physics
Delhi Technological University

Prof. S. C. Sharma
HOD
Department of Applied Physics
Delhi Technological University

ACKNOWLEDGEMENT

I am indebted to my thesis supervisor **Dr. Amrish K. Panwar**, Department of Physics, for his gracious encouragement and very valued constructive criticism that has driven me to carry the project successfully.

I would also like to express my sincere thanks to **Dr. Pawan Tyagi** who is also my branch coordinator for his help and constructive suggestions during the completion of this work.

I am deeply grateful to **Prof. S. C. Sharma**, Head of Department and all faculties of Applied Physics, Delhi Technological University for his support and encouragement in carrying out this project.

I wish to express my heart full thanks to my friends for their goodwill and support that helped me a lot in successful completion of this project.

Garima Sharma

M.Tech (NST)

2K11/NST/05

Table of Contents

List of Figures

ABSTRACT

ZnO nanorods are grown on seedless and seeded Si substrates, respectively using hydrothermal method. Horizontal and vertically aligned ZnO nanorods morphologies are observed on seedless and seeded Si substrates. The as grown ZnO nanorods are characterized by x-ray diffraction to know the phase formation, energy dispersive x-ray spectroscopy and photoluminescence measurement to investigate the quality of ZnO nanorods. Structural, elemental and luminescence characterization revealed that the as grown ZnO exhibit pure wurtzite phase of ZnO and of good quality. Surface morphology of as grown ZnO nanorods is characterized by scanning electron spectroscopy which confirms that the orientation of nanorods is horizontal on seedless substrate while on seeded substrate it becomes vertically aligned. Further, vertically aligned ZnO nanorods are grown on Cu foil and doped with $FeSO_4$ for the formation of ZnO-Fe_2O_3 flower like hybrid structure. The potentiality of such flower like hybrid structure is explored as an anode material in Li-ion battery applications.

CHAPTER-1

Introduction

Lithium-ion based batteries have been realized as the emergent powers sources for modern portable electronic devices such as laptops, mobiles, PDAs, cameras etc. Lithium-ion batteries [LIBs] offer the highest energy density among all rechargeable systems making it superior to the other materials based batteries [1-3]. The electrochemical performance of Li-ion battery is basically determined by properties of the cathode material, the anode material and the electrolyte. An extensive research is going on these three components of LIB using different materials by various research groups over worldwide. However, all these three components are essential but among these components anode host structure is major concern for intercalation of Li-ion resulting in the overall capacity of battery and the life time of battery in terms of cyclic performance. This study mainly focuses on the past and recent development of the various types of anode materials and exploitation of ZnO nanostructures in Li-ion battery as an anode material. The detail organization of the present study is as follows;

Chapter 2 gives the brief history and development of Li-ion battery, its working principle, literature review of anode materials.

Chapter 3 gives the details of experimental techniques and the working principles of different characterization techniques that have been used for the synthesis and characterizations respectively for the anode material in the present study.

Chapter 4 shows the results of different characterizations of ZnO nanostructures and their detail investigation for its use as anode material in Li-ion battery.

Chapter 5 gives the summary and future direction of the present work.

CHAPTER-2

Literature Review

2.1 History and Development of Li-ion Battery

Since lithium (Li) is a most electronegative (-3.04 V) and the lightest material (6.94 $gmol^{-1}$), therefore, it was assumed that if the Li-metal is used as an anode in battery then high energy density battery system could be feasible. In 1970 the first primary Li battery was developed using Li metal as an anode offering the high capacity and high energy density that had quickly found wide applications in portable electronic devices such as watches, calculators and implantable medical devices. The development of rechargeable batteries was started by Exxon using the TiS_2 as a positive electrode and Li-metal as a negative electrode along with the lithium perchlorate in dioxolane as the electrolyte [4, 5]. In this system, TiS_2 showed a very good stability with a layered structure for the repeated Li intercalation and de-intercalation but very soon some problems became evident related to the dendrite growth on the surface of the Li-metal electrode caused by the combination of Li-metal and liquid electrolyte. After a long term cycling, Li is deposited on the anode surface forming the dendrite which can penetrate the porous separator causing the tiny short circuit leading to the thermal runways/ fire or explosion. Therefore, the further development of rechargeable batteries system was stopped for the sake of such safety hazards. This problem was attacked by substituting the Li-metal in lithium-aluminum alloy [6]. The possibility of electrochemical formation of Li-alloys in organic electrolytes was demonstrated in 1971 [7]. After that many Li-alloys based materials have been developed

for the alternative anode electrodes. There are few issues with the use of Li-alloy based anode materials. The energy density of battery is reduced by a factor of two or three as compared to pure Li-metal electrode [8-10] and the volume changes corresponding to the insertion/extraction of Li into/from the alloy material is quite substantial (200-600 %). The substantial change in volume causes the fast degradation of alloy anode due to the cracking and crumbling. Therefore, rechargeable Li-batteries which use the Li-alloy as anode materials suffer the short cycle life. The problem related to substantial volume change was tried to solve by using the graphitic carbon as the intercalation of Li with carbon in LiC_6 composition increases only up to 10% in layer distance [11]. So, graphite became the choice for the anode material in Li-ion batteries by replacing the pure Li metal and Li-alloy material electrodes. Since the end of 1980, the combination of anode, cathode and suitable electrolyte has been emerging in Li-ion battery technology. Murphy et al [12] demonstrated the concept first time and then by Scrosati group [13]. The first Li-ion battery was commercialized by Sony in the early 1990 [14].

2.2 Working Principle of Li-ion Battery

A Li-ion based battery mainly consists of three components: a positive electrode, a negative electrode and an electrolyte (solution or solid-state) containing a dissociated salt separated by a micro-porous membrane which is called separator. Figure 2.1 shows the schematic representation of working principle of Li-ion battery in which Li-ions shuttle between anode and cathode electrodes through the electrolyte. Before using the Li-ion battery one should charge the battery in that process, Li-ions are extracted from the cathode and passes through the electrolyte and separator and then finally intercalated in anode electrode

material. Simultaneously, electrons of equivalent charge are released by cathode travelling in external circuit and then adopted by the anode electrode. The reverse phenomenon takes

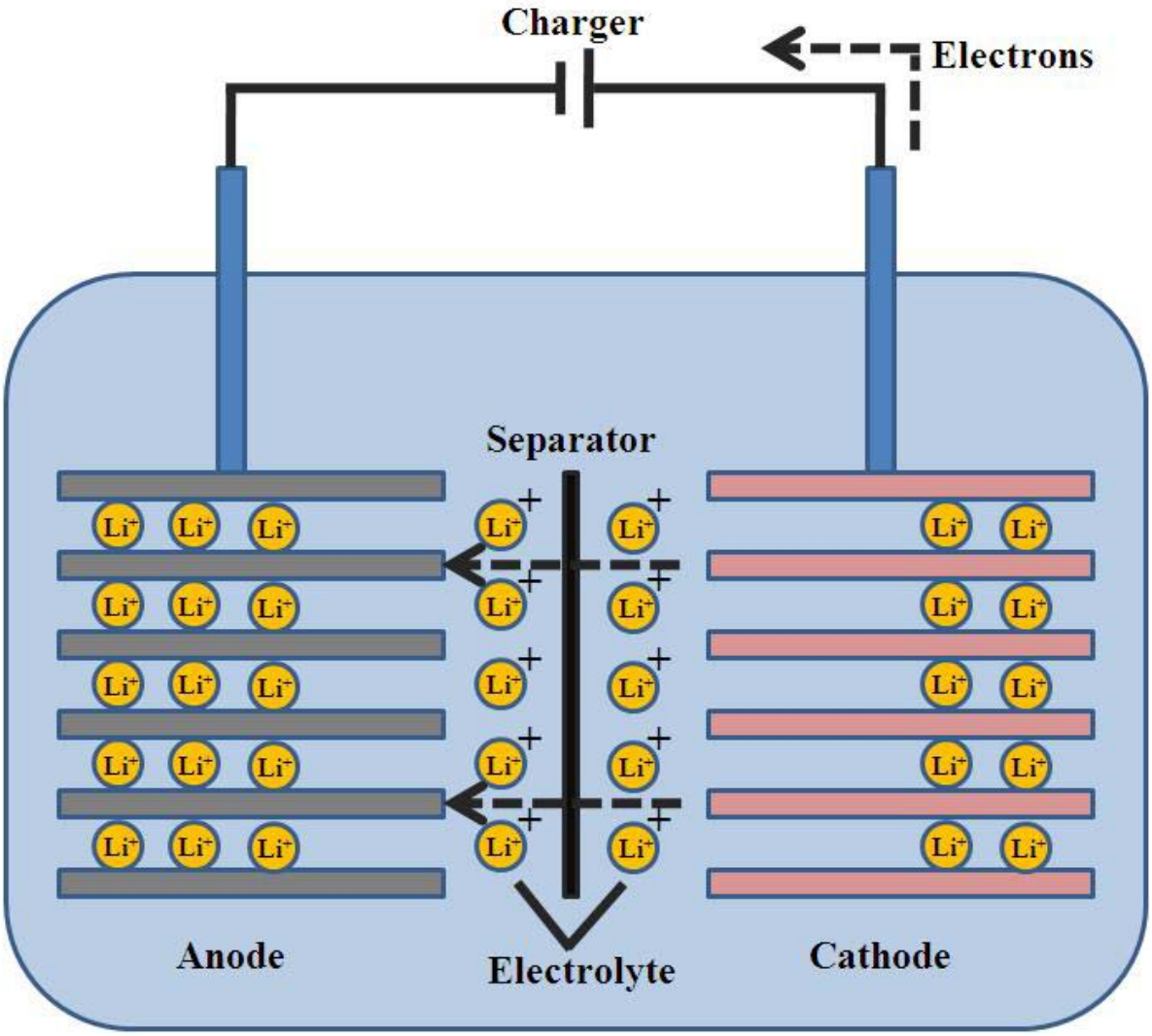

Figure 2.1 Schematics representation of working principle of Li-ion battery under charging process.

place when we take the power output (discharging process) from the Li-ion battery. To get the high performance of Li-ion battery i.e. high cycling efficiency and long cycles life, it is

highly desirable that the degradation in crystal structure of both the electrodes should be as low as possible during the movement of Li-ion between the electrodes. The design of the Li-ion battery system should be such that one can get the maximum operating voltage (V_c) that can be realized by the careful selection of pair electrode materials. To get the high V_c the work functions of anode and cathode should be lower (Φ_a) and higher (Φ_c) respectively. The open circuit voltage V_{OC} of the cell can be estimated be the following formulae;

$$V_{OC} = \left(\frac{\Phi_a - \Phi_c}{e} \right) \tag{2.1}$$

where '*e*' is the electronic charge.

Carbon with a potential of 0-0.8 V versus Li metal is highly desirable for anode material in Li-ion battery whereas cathode materials can be opt from the spinel $LiMn_2O_4$, layered $LiCoO_2$ and $LiNiO_2$ which have discharge potential of the order of 4V versus Li-metal. A L-ion battery with the combination of low potential anode and the high potential cathode can deliver a voltage up to 3-4 V, which is three times higher than the other materials based batteries (Ni-Cd or Ni-MH).

2.3 Various Types of Anode Materials

Since the rechargeable Li-ion batteries using the pure Li-metal as electrode were not feasible in early trials due to the safety problem. So, people started to search the materials in which Li-ion can be inserted or extracted without affecting much its crystal structure. The most common materials for Li-intercalation are carbon in both forms graphitic or non graphitic and suitable alloying metals eg. Sn, Al, Pb, Bi, Sb, As etc. Some oxides such as $Li_4Ti_5O_{12}$ and Li perovskites with relatively low potential (1.0-1.5V) can also be used for anode material. Mainly three basic requirements are considers for choosing the anode

materials: the potential of Li insertion and extraction in the anode versus Li must be as low as possible, The capacity of anode material for Li insertion must be as high as possible and the crystal structure should not damage by repeated insertion and extraction of Li-ions [15]. Here we are briefly describing the few anode materials.

2.3.1 Carbon Based Materials

Carbon has been remaining the commercialized anode material in industry for Li-ion battery. During the development of Li-ion battery, initially, graphite was used as an anode host but attempt was not successful due to the disintegration of anode. The reason was discovered as poorly crystalline carbons were less sensitive to the electrolyte decomposition. Further, the feasibility was demonstrated with modest capacities as compare to as expected with carbon [16]. The first commercialization of Li-ion battery using the non-crystalline carbon anode was done by Sony company.

2.3.1.1 Structure Exhibited by Carbon: Graphitic Form

Carbon material covers a wide range of structure, texture and properties. Normally, carbon material is divided into three categories: graphitic, non graphitic (hard carbon) and soft

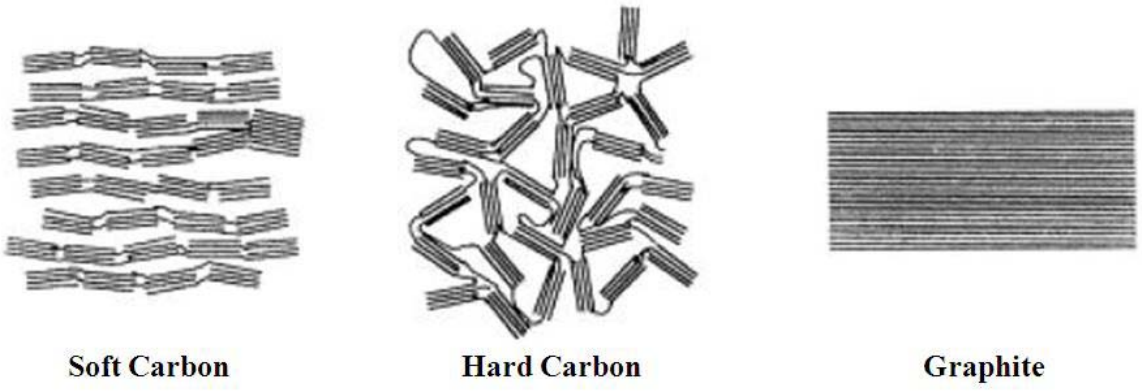

Figure 2.2 Schematics of different forms of carbon.

carbon. Figure 2.2 shows the schematic representation of these three classes of carbon material [17]. Pure graphite exhibits ABAB type of structure that consists of hexagonal planes of carbon stacked along c-axis. The space group of graphite is Pb3/mmC with a=b=2.46 Å and C=6.70 Å and a lateral shift occurs if we go from A layer to B layer. The schematic representation of structure of pure graphite is shown in Figure 2.3. Other graphite stacking like ABCA or ABAC are also possible due to stacking faults [18].

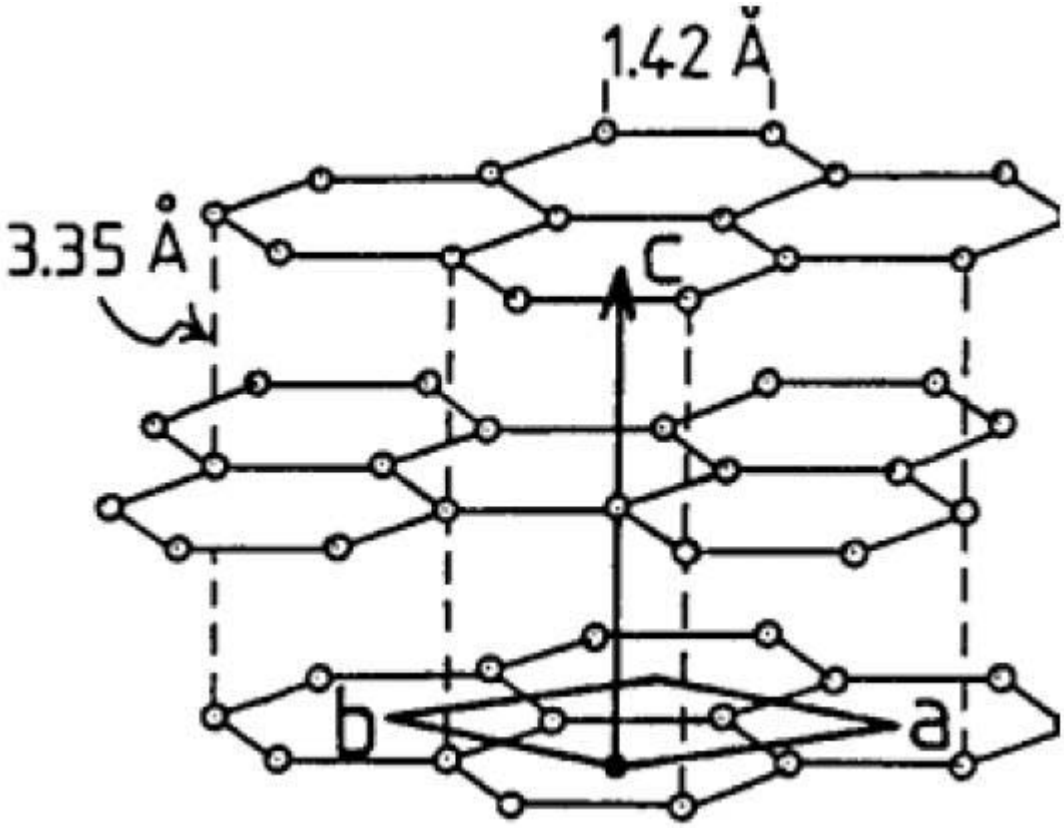

Figure 2.3 Hexagonal structure of graphite showing the ABAB stacking of honeycomb carbon layers

There are several forms of carbon that can be compatible to the Li-ion battery and their structure strongly depends on the synthesis procedure. Graphitic carbon can be synthesized by delivering the heat treatment to the soft carbon precursors above the 2400 ºC which results in well graphitized material. Pyrolysis of organic precursors at 700 ºC results the

hydrogen containing carbon. In early stage, organic precursors were pyrolyzed below 600 ^{o}C by which organic compounds decomposes and emits the gases containing the carbon eg. CO and CH_4 while remaining carbon atoms condense into planar aromatic structure. If the decomposition of organic precursor results the semifluid state then it is easy to align these planar sheets in more parallel fashion resulting the easy graphitization upon heating to a very high temperatures. This is called the 'soft' or graphitizable carbon. If the organic precursors are easily cross-linked and semifluid state does not occur then planar aromatic structure cannot align. These carbon materials are not easy to graphitize at high temperature, therefore, called the 'hard' or non-graphitizable carbons.

2.3.1.2 Carbon Nanotubes

The major disadvantage of Li-ion batteries is their low power density due to the high polarization at high charge-discharge rates. The high polarization causes due to the slow Li ion diffusion rate, poor electrical and thermal conductions in the electrode and at electrode-electrolyte interface. These problems can be overcome by choosing the electrode material that exhibits large surface area and high electrical/thermal conduction. Electrode materials in nano regime offer many advantages over conventionally available: (i) reversible Li intercalation and its extraction without affecting much the electrode material, (ii) increment in insertion/removal rates of Li due to the short transport path, (iii) increased electron transport properties (iv) enhanced contact area with the electrolyte, decrement in volume changes due to intercalation [19]. Therefore, carbon materials can be formed in a Varity of nano structures, however, carbon nanotubes (CNTs) has been most studying as an additive for both anode and cathode electrodes or as a replacement material for anode electrode. CNT is a 1D material with a length-to-diameter ratio$\geq$ 1000. CNTs are envisioned as a

cylinder composed of rolled grapheme sheets around a central hollow core. Recent development on Li-ion batteries involved the synthesis of hybrid structure of CNTs and Li storage materials.

2.3.1.3 Lithium Intercalation of Carbon Materials

During the charging process Li extracted from the cathode and inserted into anode host made of carbon material resulting the intercalation of Li into carbon layers by forming LiC_6 with the following reaction.

$$Li^+ + 6C \longrightarrow LiC_6 \qquad (2.2)$$

The theoretical capacity of graphite has been reported as 372 $mAh.g^{-1}$ (850 $mAh.cm^{-3}$). The intercalation of Li ion to the carbon materials is different depending on its graphitic, non graphitic and hydrogen contained carbons. MesoCarbon MicroBeads (MCMB) is a graphitic form of carbon in which during the intercalation, for the first cycle the charge consumed exceeds the theoretical capacity. This is due to the side reaction which involves the decomposition of electrolyte. Electrolyte decomposition attributed to the exfoliation of graphite resulting the irreversible capacity. Careful selection of electrolyte can avoide such catastrophic effects on the electrodes. For the first intercalation, the side reaction induces the formation of passivation layer on the surface of electrode, called the solid electrolyte interface (SEI). The SEI layer is electronically insulating but ionically conducting that prevents the further decomposition of electrolyte during the ionic transfer in the solution. The formation of SEI layer provides the stability and cyclability of the carbon electrode.

The behavior of Li insertion in hard carbons is different from the graphitic one. In contrast to the graphitic, the hard carbon shows the continuous charge/discharge curves between 1.2 and 0.2 V associated with Li intercalation [20] rather than the staging plateau. People

believed that the inserted Li in hard carbon fills the micro-pores in carbon by clustering of Li. Hard carbon consists of single layer of carbon sheets to which of both sides Li can be absorbed leading to a more Li per carbon than in the intercalated graphite thus yielding the theoretical maximum capacity of Li_2C_6 or 740 $mAhg^{-1}$.

Hydrogen containing carbon can provide the high Li intercalation capacity of the order of 800-900 $mAhg^{-1}$.indicating that the hydrogen plays a crucial role in the mechanism of Li insertion. It has been observed that the reversible capacity can be increased with the increase of H/C atomic ratio in this material which indicates that hydrogen atom favors to bind the Li ions in its vicinity. The Li-ion transfers its few 2S electrons to the hydrogen atom forming the H-C bond which causes the change in relative atomic positions of H and C atoms. The disadvantage of hydrogen-carbon anode electrode material is that they do not maintain their large capacity over long term cycling [21, 22].

The carbon materials are still investigated under intense research to improve their specific capacity and long cycle life. In addition to the carbon based materials, there are other materials such as Li-alloys, intermetallic alloys; metal oxides such as tin oxide and Spinel lithium titanium $Li_4Ti_5O_{12}$ (LTO) have also been explored as an anode material for Li-ion battery system.

2.3.2 Fe_2O_3 as an Anode Material

Recently, hematite (Fe_2O_3), the most stable phase of iron oxide has drawn a considerable attention in nano form as the promising anode material for the Li-ion battery system because of its high theoretical capacity (1007 $mAhg^{-1}$) and abundance in nature [23-28]. However, the substantial volume-change and low electronic conductivity of this material in the process of lithiation and delithiation hinder the improvements in cycling performance

and rate capability [29]. An approach for reducing the volume change can be possible by synthesizing the Fe_2O_3 in nano form whereas Fe_2O_3 nanostructures growth on metallic substrate can be beneficial for rate capability because of the direct contact between Fe_2O_3 and current collector, a short diffusion path for ions and electrons, large surface area for electrolyte and good strain adoption. Few efforts have been attempted for the synthesis of Fe_2O_3 with various morphologies [30-33]. But it is still demanding to grow the Fe_2O_3 nanostructures on metal substrates that can used in designing the high performance electrochemical energy storage devices. Therefore, one can think about such material which can easily be grown in various morphological nanostructures as well as can be used as a template to grow the Fe_2O_3 nanostructures. Zinc oxide can be one of the best choices for such template.

Zinc oxide (ZnO) has created a substantial interest in the research community due to its direct wide band gap (~ 3.2 eV) and large exciton binding energy (~ 60 meV) [34-36]. Its wide band gap facilitates to make optoelectronic devices in the ultraviolet region whereas large exciton binding energy helps to increase the efficiency of these devices at room temperature because the dissociation energy (i.e. binding energy ~ 60 meV) of formed excitons is much larger than the room temperature energy (~ 25 meV), sustaining them for longer time before the recombination. ZnO is not a new material in semiconductor field as research has been carried out on this material over a period back to 1960 but it was not as progressive as it is in recent years. In very past few years the studies related to its structure [37], vibrational properties [38], optical properties [39] and growth [40] have been reported. In terms of device, Au Schottky barriers [41], light emitting diodes [42] and ZnO/ZnSe n-p junctions [43] were also fabricated. The renewed interest for research on this material is

fueled by the availability of high quality substrates, the possibility of formation of p-type ZnO [44-50] and observation of ferromagnetic behavior in ZnO when doped with transition metals [51,52]. The possibility of p-type ZnO brought great interest to researchers for fabricating ZnO based homojunctions. The main hindrance to achieve this goal is to have reproducibility in synthesizing p-type ZnO with large carrier concentrations. In recent years, intense research by different groups has been focused to grow novel nanostructures ranging from nanowires to nanobelts and nanosprings [53-56]. The growth of nanostructures of ZnO again fueled the renewed interest on this material in exploring the possibility of fabricating the optoelectronic devices in nano regime [57, 58].

2.3.3 Properties of ZnO

In this section, brief introduction of various properties such as structural, optical defects and doping of ZnO are presented.

2.3.3.1 Crystal Structure

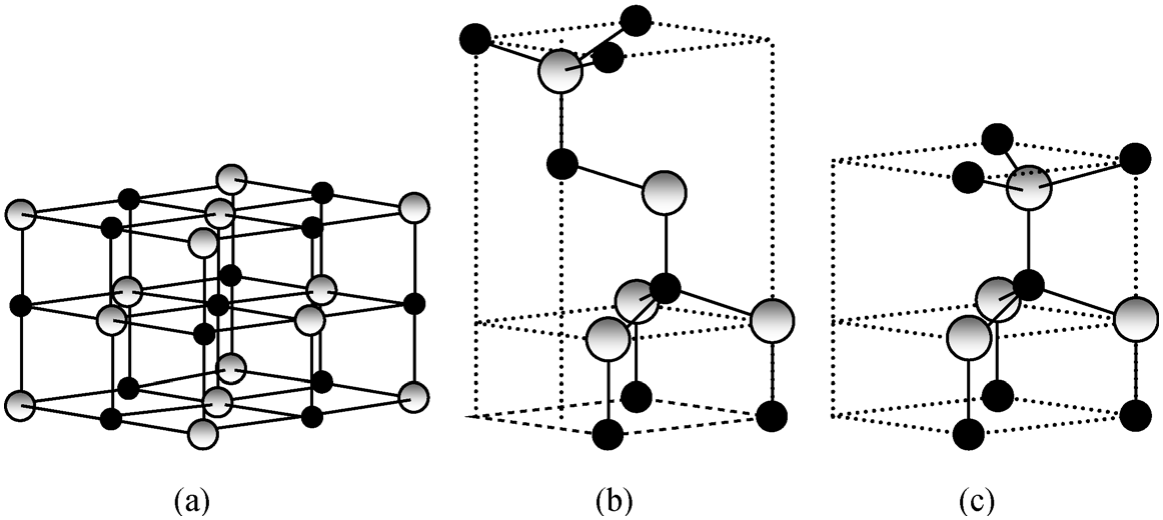

Figure 2.4 Three possible types of crystal structures for ZnO: (a) rocksalt, (b) cubic zinc blende and (c) wurtzite.

ZnO exists in one of three crystal structures: wurtzite, cubic zinc blende and rocksalt. Figure 2.4 shows the three possible crystal structures of ZnO [59]. Thermodynamically most stable phase of ZnO at ambient condition is wurtzite. The zinc blende structure of ZnO can be realized when it is grown on cubic substrates while the rocksalt structure can be realized under high pressure.

The wurtzite phase of ZnO has a hexagonal unit cell with lattice parameters, a and c. The space group of ZnO is C^4_{6v} or $P6_3mc$. Wurtzite structure of ZnO is composed of two interpenetrating hexagonal closed pack (hcp) sublattices. Each sublattice consists of one type of atom displaced with respect to other sublattice along the three fold c-axis by the numerical value of u = 3/8 in fractional coordinates. Each sublattice includes four atoms per unit cell and every atom of one kind is surrounded by four atoms of the other kind, or vice versa, which are coordinated at the edges of the tetrahedron. In practice, the wurtzite crystal structure of ZnO deviates from the ideal arrangement, by changing the c/a ratio or u value. When c/a ratio increases, the u value decreases in such a way that the four tetrahedral distances remain nearly constant through a distortion of tetrahedral angles due to long range polar interaction. The following relation correlates the c/a ratio and u parameter in wurtzite crystal,

$$u = \left(\frac{1}{3}\right)\left(\frac{a^2}{c^2}\right) + \left(\frac{1}{4}\right) \tag{2.3}$$

Figure 2.5 shows the the unit cell of ZnO in wurtzite phase. The bonding between Zn and O at the edge of tetrahedral is covalent with sp^3 hybridization. ZnO shows substantial ionic character whose ionicity resides at the boarder line between ionic and covalent semiconductors. In addition to this, ZnO shows polar nature along c-axis due to the

arrangement of positively charged Zn-(0001) and negatively charged O-$(000\bar{1})$ surfaces.

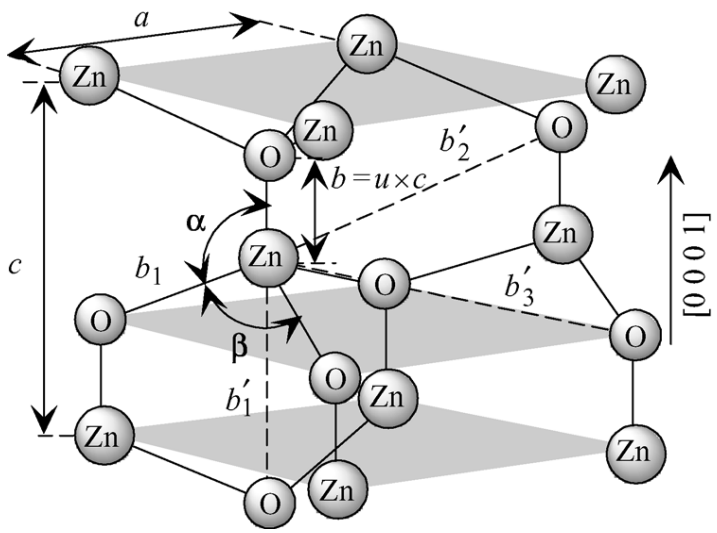

Figure 2.5 Unit cell of ZnO in wurtzite phase.

The lattice parameters of ZnO are determined by the following four factors: (i) free-electron concentration acting via deformation potential of a conduction band minimum occupied by these electrons, (ii) concentration of impurities and defects and the difference of their ionic radii with respect to substituted matrix ions, (iii) extrinsic and intrinsic strains, and (iv) temperature. The lattice constants for the wurtzite ZnO range from 3.2475 to 3.2501 Å for the 'a' parameter and from 5.2042 to 5.2075 Å for the 'c' parameter. The c/a ratio and u parameter vary from 1.593 to 1.6035 and from 0.383 to 0.3856, respectively.

2.3.4 Growth of ZnO

ZnO is grown in bulk, thin film and various nanostructure forms. Thin films and nanostructures of high quality are required to realize its application in optoelectronic devices. ZnO thin films have been grown on different substrates by various techniques such as: sputtering [60], molecular beam epitaxy [61], pulsed laser deposition [62], chemical

vapor deposition [63], spray pyrolysis [64] and sol-gel [65]. In order to grow epitaxial ZnO films with reduced strains and dislocation density, lattice matched substrates are required. Sapphire with (0001) orientation is preferred to grow the epitaxial ZnO film. Apart from sapphire other substrates like glass and quartz are frequently used to grow the polycrystalline ZnO film. Indium Tin Oxide (ITO) coated glass substrate is also frequently used to grow the ZnO film for the device fabrication.

Growth of ZnO nanostructures such as nanowires [66] nanorods [67] nanobelts [68] and nanotubes [69] have become an area of intense research due to their potential for applications in novel devices. Different synthesis routes such as non-catalytic thermal evaporation [70] chemical vapor deposition [71] laser ablation [72] electrochemical process [73] and chemical solution or hydrothermal method [74,75] have been employed to grow ZnO nanostructures. The chemical solution method has attracted great interest because this method allows to grow the nanowires and nanostructures at low temperatures. In addition to this, chemical solution method is economical, nontoxic and requires vacuum less environment method to grow ZnO nanostructures.

CHAPTER-3

Experimental Section

3.1 Introduction

This chapter presents brief description of synthesis of ZnO nanostructures which have been used in the present work. Apart from this, different characterization and measurement techniques, which are used to study various properties of the samples are also presented in this chapter. ZnO nanostructures have been grown by chemical solution method. Structural characterizations of nanostructures have been carried out using X-ray diffraction. Shape and size of nanostructures and the orientation of planes inside the nanostructures have been studied by transmission electron microscopy and high resolution transmission electron microscopy, respectively. Surface morphology and oriented growth of ZnO nanowires have been investigated by scanning electron microscopy. Photoluminescence measurement has been carried out by photoluminescence spectrometer.

3.2 Growth of ZnO Nanostructures

In the present study ZnO nanostructures were grown by two methods; hydrothermal and partially sacrificed template.

3.2.1 Hydrothermal Method

Hydrothermal solution technique is used to grow ZnO nanostructures. In this technique, for growing nanostructures of a particular metal oxide, inorganic compound of that metal, generally acetate or nitrate is dissolved in water. Organic solvent like alcohols are also used

to dissolve the metallic inorganic compound and to form the complex compound of that metal which can easily be decomposed at low temperatures. Alcoholic solvent provides the reduced atmosphere in the solution. The heating of solution of metallic inorganic compound in an organic solvent at low temperature < 200 °C results in crystallizing the metal oxide at various places in the matrix of solution. The growth of nanostructures in the hydrothermal solution process is governed by various parameters like: temperature, water content, concentration of reactant constituents, type of functional group attached in the solvent and PH of the solution. Variation of any growth parameters results in a different shape and size of the nanostructures. For the oriented growth of nanorods on a substrate, seeds are used which act as nucleation centers for the aligned growth of nanorods. Surfactants like amines are also used to form the anisotropic growth of nanostructures. In the present work, this hydrothermal solution method is used to synthesize the ZnO nanostructures.

ZnO nanorods have been grown on seedless and ZnO seeded substrates by solution method. Aqueous solution of Zn (Ac).$2H_2O$ has been used for preparing seeds on desired substrates. For growing ZnO nanorods on seedless and seeded glass substrate, equimolar (0.1 M) aqueous solution of Zinc nitrate hexa-hydrate (Zn (NO_3).$6H_2O$) and hexamethylenetetramine (HMT). The substrates are dipped vertically in the solution of Zn (NO_3).$6H_2O$ and HMT in a closed jar and the jar is kept in an oven at 95 °C. ZnO nanorods have been grown on seedless substrate for 16 hours and on seeded substrates for 4 hours and 16 hours. After the growth of ZnO nanorods on glass substrate it is washed with deionized water and dried by keeping the samples on hot plate for few minutes.

3.3 Synthesis of Anode Material (Fe_2O_3) for Li-Ion Battery

The grown ZnO nanorods were immersed in the aqueous solution of ferrous sulphate ($FeSO_4$) by varying the molarities from 10 mM-0.2 M for 5, 10, 15, 20, 25 and 30 minutes. After that samples were washed with distilled water and dried and then heated at 350 ºC for 30 minutes in inert atmosphere. The resulting ZnO-Fe_2O_3 may further be used as anode material for Li-ion batteries application.

3.4 Characterization Techniques

The characterization of ZnO nanostructures has been carried out by various techniques. Brief descriptions of these techniques are given in the following subsections.

3.4.1 Structural, Morphological and Elemental Characterization

3.4.1.1 X-Ray Diffraction

X-ray diffraction is a powerful technique for the investigation of crystal structure of a material. Apart from the crystal structure of the material, it is also used for the chemical analysis, stress measurement, study of phase equilibria, and calculation of particle/crystallite size and preferred orientation of one crystal or ensemble of orientation in polycrystalline aggregate. In XRD, the collimated beam of X-rays impinges on the crystal planes and intensity of diffracted X-rays are measured. Crystal is a periodic arrangement of atoms in three dimensions, therefore, capable of diffracting the X-ray radiation impinging upon it.

Figure 2.5 shows periodic arrangement of atoms in a crystal. The periodic arrangement of atoms in a two dimension may be considered as an atomic plane. The crystal can be considered as composed of many sets of atomic planes. Each plane is represented by (hkl), known as miller indices of the plane. These planes are separated by a distance d, known as

interplanar spacing. When X-ray beam impinges on the specimen at an incident angle θ then atoms in the specimen scatter the X-rays. If the scattered rays are in phase, they interfere constructively and a diffracted beam with a significant intensity is obtained in a specific direction. Bragg developed a relation among the incident X-rays wavelength (λ),

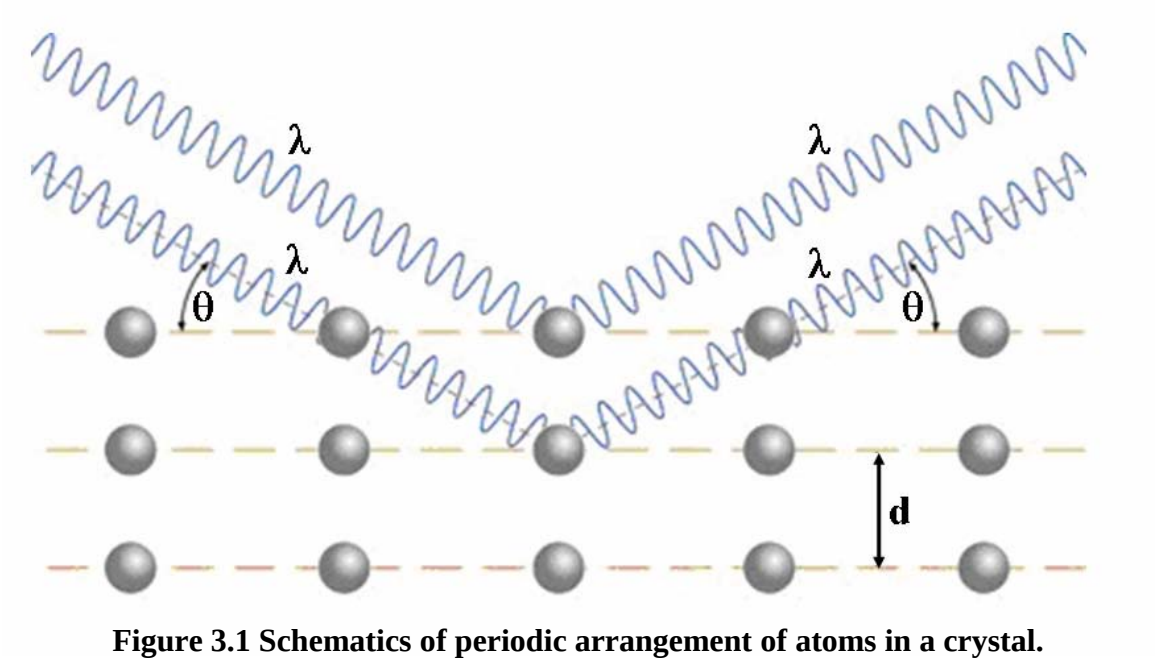

Figure 3.1 Schematics of periodic arrangement of atoms in a crystal.

interplanar spacing (d_{hkl}) and incident angle (θ_{hkl}) of X-rays, known as Bragg law, which is given as;

$$2d_{hkl}\sin\theta_{hkl} = n\lambda \tag{3.1}$$

where n is an integer number called, order of reflection.

The arrangement of X-ray source, specimen and detector in the geometry of an X-ray diffractometer is shown in figure 2.6. In this geometry, the angle between the projection of X-ray source and detector is 2θ and the X-ray diffraction patterns produced with this geometry are known as θ-2θ scans.

In the XRD pattern, broadening of diffraction peak is related to crystallite size and it can be estimated by measuring the full width at half maximum (FWHM) of the peak intensity. Broadening of diffraction peak arises mainly due to three factors: instrumental effects,

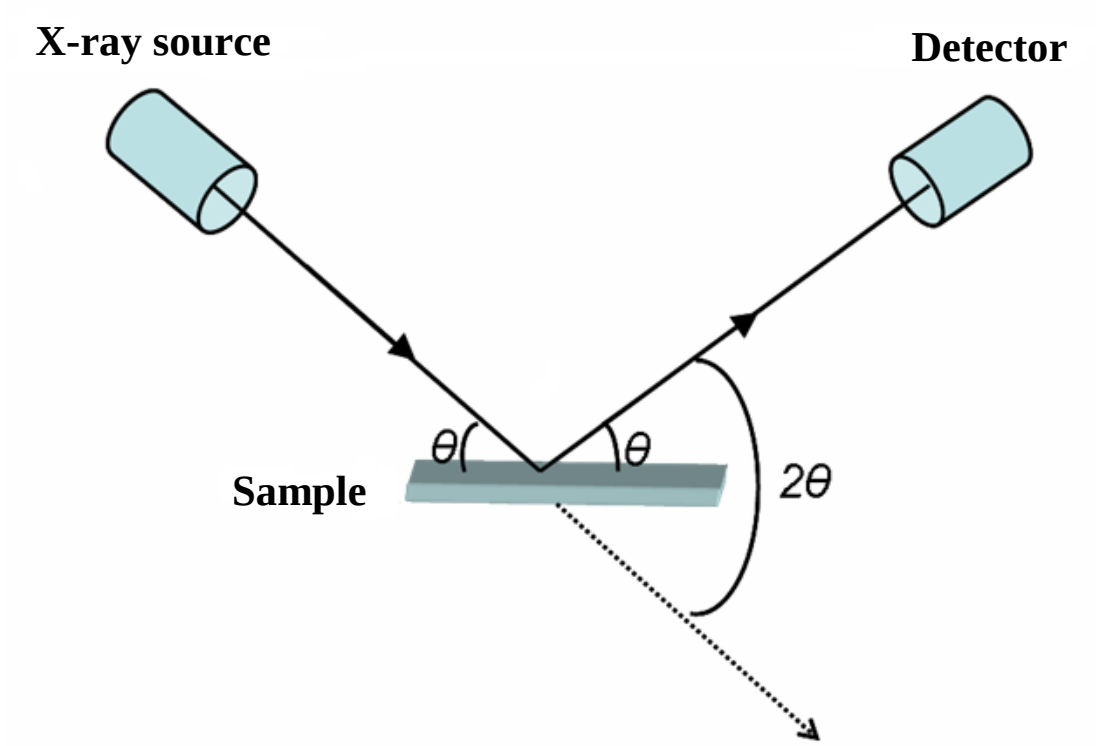

Figure 3.2 Schematics of an arrangement of X-ray diffractometer.

crystallite size and lattice strain. Broadening due to instrument can be estimated by measuring the diffraction pattern of well annealed (i.e. strain free) standard powder whose crystallite size is so large that it does not cause any broadening. Subtraction of instrumental broadening from the peak broadening leaves the broadening of peak only due to crystallite size and strain. Scherrer derived a relation for broadening ($\beta_{crystallite}$) of X-ray diffraction peak due to only small crystallite sizes which is given as;

$$\beta_{crystallite} = \frac{k\lambda}{t\cos\theta_B} \tag{3.2}$$

where λ is the wavelength of the incident X-rays, θ_B is the Bragg angle, t is the average crystallite size measured in a direction perpendicular to the surface of the specimen and k (~ 0.89) is a constant.

In the present work, X-ray diffraction measurement is performed using Brukar made D-08 X- ray differacto-meter with Cu$K_{\alpha 1}$ radiation (1.540 Å). The X-rays are generated by applying 40 mA current and 45 KV voltage on anode material Cu in conjunction with Ni filter to attenuate $CuK_{\alpha 2}$ and CuK_{β} radiation**.**

3.4.1.2 Scanning Electron Microscopy

Scanning electron microscopy (SEM) is a powerful technique for observing the surface morphology of a specimen at very high magnifications. SEM magnifications can be more than 300,000 X and gives the resolution of the order of few nm. SEM is often used for the analysis of cracks and fractured surfaces, physical defects on the surfaces, surface morphologies, shape of the grains and orientation of nanostructures etc. In SEM, electrons are generated by thermionic emission from a metal filament. A system of electrical and magnetic field optics is used to focus the electron beam on the sample surface. These bombarding electrons, also referred to as primary electrons, dislodge electrons from the specimen itself. The dislodge electrons are attracted and collected by a positively biased grid or detector. For producing the SEM image, the electron beam is swept across the area over the surface of the sample and the signals are then amplified, analyzed, and translated into images of the topography of the sample. The sample surface must be electrically conducting, otherwise electron beam would charge up the sample surface. Insulating samples are given a coating of conducting material, generally Gold (Au), before SEM

imaging. In the present work, Hitachi make S-3700N SEM is used to observe the surface morphology, distribution and orientation of ZnO nanorods.

3.4.1.3 Energy Dispersive x-ray spectroscopy

An analytical technique used for the elemental analysis or chemical characterization of a sample is term as energy dispersive x-ray spectroscopy which relies on the investigation of an interaction of some source of X-ray excitation and a sample. The fundamental principle on which EDS works is that each element has a unique atomic structure allowing unique set of peaks on its X-ray spectrum. When a high-energy beam of charged particles such as electrons or protons or a beam of X-rays is focused into the sample, then there will be a stimulation of the emission of characteristic X-rays from a specimen. All elements from atomic number 4 (Be) to 92 (U) can be detected in principle, though not all instruments are equipped for 'light' elements ($Z < 10$).

In ground state, an atom within the sample contains electrons in discrete energy levels. When an incident beam falls on the sample it may excite an electron from inner shell, ejecting it from the shell while creating a hole in place of electron. Now an electron from an outer, higher-energy shell then fills that hole. The energy difference between the higher-energy shell and the lower energy shell may be released in the form of an X-ray. The energy and number of the X-rays emitted from a sample can be measured by an energy-dispersive x-ray spectrometer. Since the energy of the X-rays are characteristic of the difference in energy between the two shells, and of the atomic structure of the element from which they were emitted, this allows the elemental composition of the specimen to be measured.

3.4.3 Photoluminescence Measurement

Figure 3.3 shows schematic diagram of measurement setup of photoluminescence.

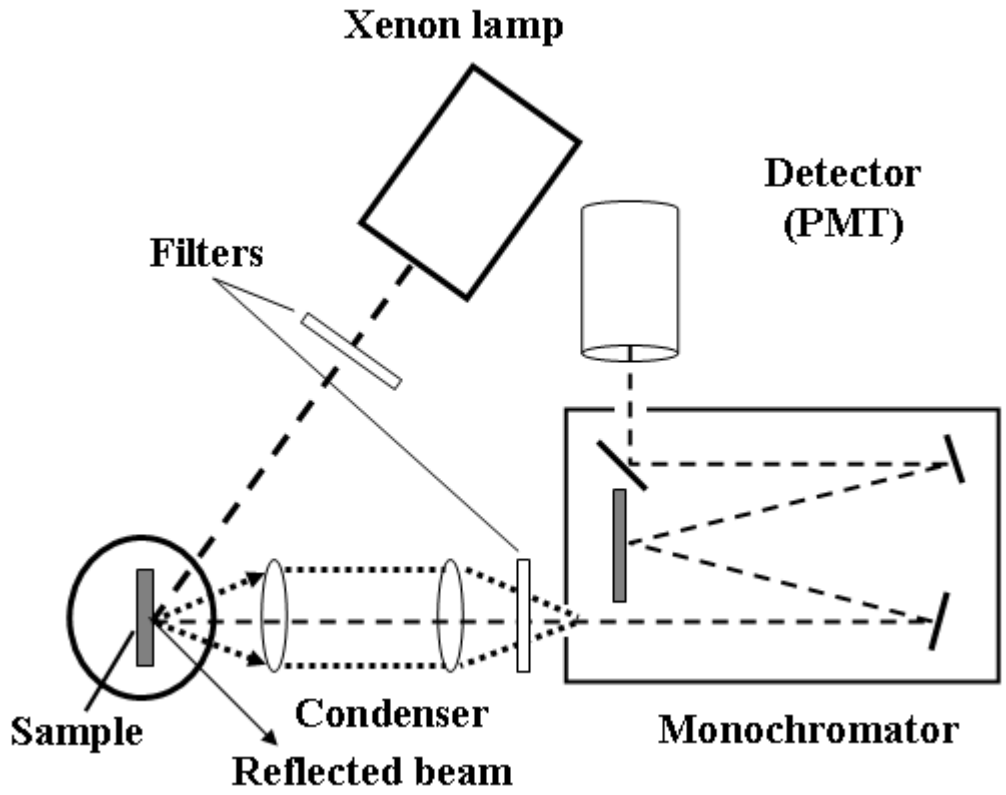

Figure 3.3 Schematic diagram of measurement setup of photoluminescence.

Photoluminescence (PL) is a process in which material absorbs incident photon energy and then re-radiates photons. When the material is irradiated with the light having energy greater than the optical band gap of the material, atoms or molecules inside the material absorbs the incident photons and get excited to a higher energy states. After a very short time interval, these excited atoms or molecules come to the ground states via radiative emission. This radiative emission from the material is called the luminescence and gives the information about the characteristics of the material. In case of semiconductors, electrons

get excited from valence band to conduction band. Few of the excited electrons may also form electron-hole pair, called excitons, which upon radiative recombination gives energy nearly equal to the band gap energy. In semiconductors, intrinsic and extrinsic defects forms energy levels within the band gap, therefore, few of the excited electrons come to the ground states via defect states via non-radiative or radiative process and emitting light of energy less than the band gap energy. The luminescence energy, less than the band gap energy is a characteristic of a particular defect and gives the information about the nature of the defect.

In the PL measurement setup Xenon lamp is used as a source of wide range of wavelength. Filter is used to select a particular excitation wavelength. When the light of particular excitation wavelength is incident on the sample, it gives the luminescence in the reflected light. With the help of optical arrangement, the intensity of reflected light is measured as a function of wavelength by a photomultiplier tube.

In present investigation, photoluminescence spectrometer (specrtofluorometer: model-3-11) has been used to carry out PL measurement of ZnO nanostructures using excitation wavelength of 325 nm obtained from Xenon lamp.

CHAPTER-4

Results and Discussion

This chapter presents the characterizations of ZnO nanorods. ZnO nanorods are grown on seedless and seeded Si substrates by hydrothermal method. Further, the potentiality of these nanorods is explored by growing the Fe_2O_3 nanostructures over ZnO nanorods template as Li-ion battery anode material. In addition, ZnO nanorods samples are also prepared on Cu foil for making the anode material by doping these nanorods with ferrous sulphate. The structural, morphological characterizations and elemental analysis are carried out using XRD, SEM and EDS, respectively. Photoluminescence spectra is also performed to investigate the quality of grown ZnO nanaorods.

4.1 ZnO Nanorods on Si Substrate

4.1.1 X-Ray Diffraction

Figure 4.1 shows XRD patterns of ZnO nanorods grown on seedless Si substrate. XRD exhibits a strong reflection corresponding to (100) plane at 31.8º value of 2θ, which is one of the planes of wurtzite hexagonal phase of ZnO. It indicates that the ZnO nanorods grown on seedless substrates have strong orientation along (100) direction. In addition, two more reflections corresponding to (002) and (101) planes are also observed at 34.6º and 36.4º values of 2θ, respectively. However, the intensities of (002) and (101) planes is lower as compared to (100) planes. Therefore, XRD data concludes that the as grown ZnO nanorods on seedless substrate are not oriented along c-axis or vertically aligned to substrate [76].

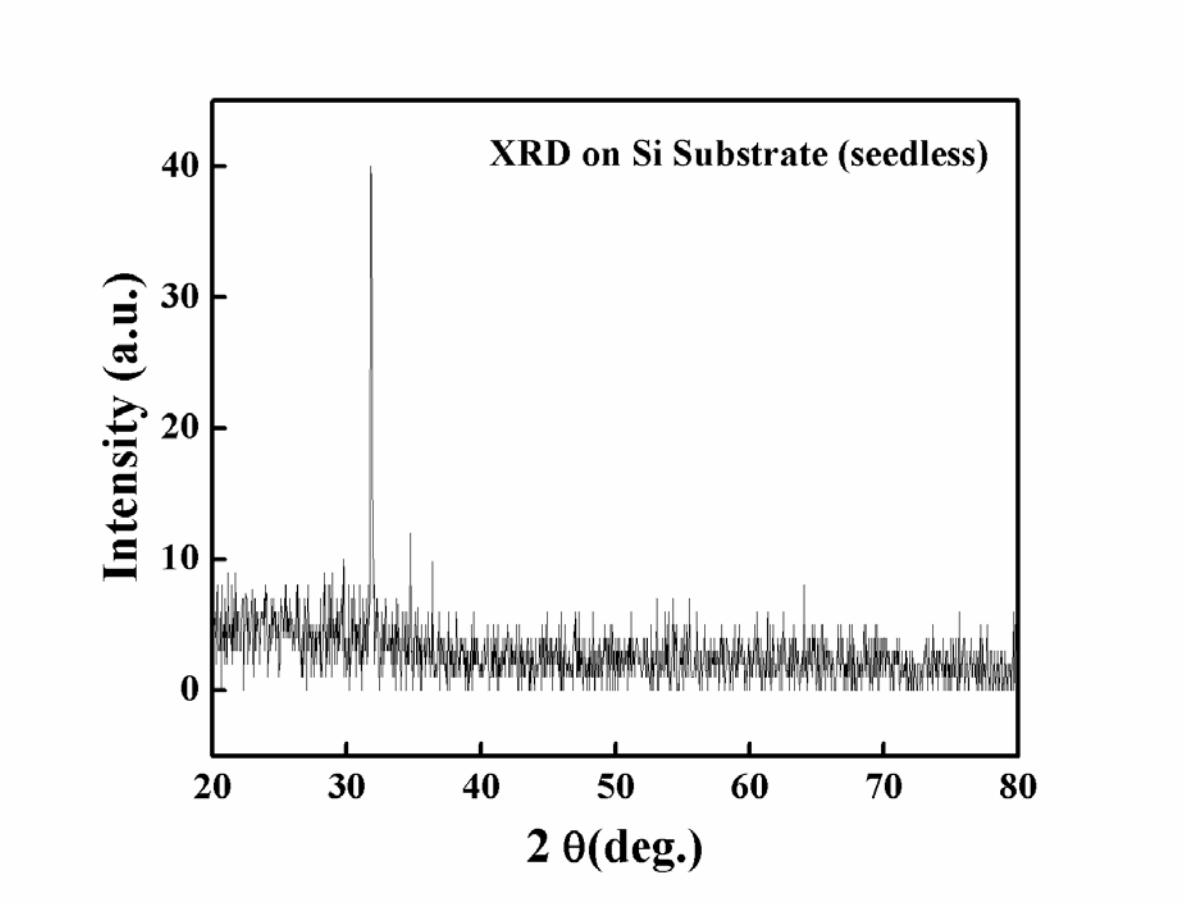

Figure 4.1 X-ray diffraction pattern of grown ZnO nanorods on seedless Si substrate.

Since the vertically aligned ZnO nanorods can be the good choice for Li-ion battery application as compared to horizontally aligned rods because vertical alignment can provide the large exposed surface area and regular porosity. It is well known that the ZnO nanorods may aligned vertically by depositing the seeds over the desired substrate as these seeds act as a nucleation sites for vertically grown nanorods. Therefore, Si substrate is prepared by depositing the ZnO seeds by employing the procedure as described in 4.1 section. After depositing the seeds the ZnO nanorods are grown over using the same precursor as in case

of without seeds. Figure 4.2 shows the XRD pattern of as grown ZnO nanorods on seeded Si substrate.

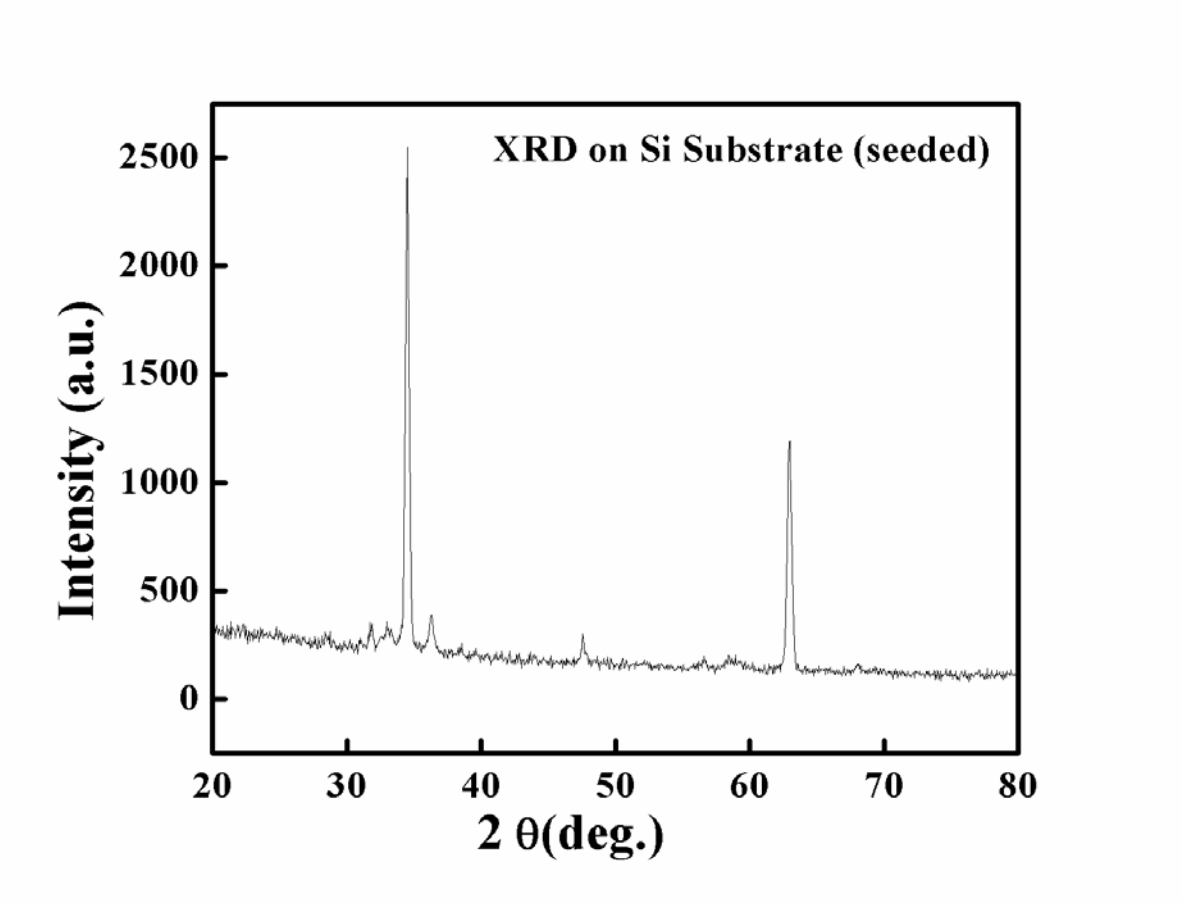

Figure 4.2 X-ray diffraction pattern of grown ZnO nanorods on seeded Si substrate.

XRD of grown ZnO nanorods on seeded substrate exhibit a strong reflection corresponding to (020) plane at 34.4º value of 2θ, which is most prominent plane especially for vertically alignment in wurtzite hexagonal phase of ZnO. It indicates that the ZnO nanorods grown on seeded substrates have strong orientation along (002) direction indicating that the as grown ZnO nanorods are vertically aligned. In addition, two more reflections corresponding to (100) and (101) planes are also observed at 31.8º and 36.2º values of 2θ, respectively.

However the intensities of (100) and (101) planes is much lower as compared to (002) planes. Therefore, XRD data concludes that the grown ZnO nanorods on seeded substrate are strongly oriented along c-axis or vertically aligned to substrate.

4.1.2 Scanning Electron Microscopy

The morphological and distribution studies of grown ZnO nanorods over seedless and seeded Si substrate are carried out by scanning electron microscopy (SEM). Figure 4.3 shows the SEM image of grown ZnO nanorods at seedless Si substrate.

Figure 4.3 SEM image of grown ZnO nanorods on seedless substrate indicating the horizontal alignment of nanorods.

The SEM image of ZnO nanorods grown on seedless Si substrate as shown in Figure 4.3 indicates that the alignment of rods is horizontal i.e. not vertical which supports the XRD data for seedless substrate. The diameter of nanorods is observed within the range of 150 nm to 200 nm where as length of nanorods is observed within the range of 1-2 micron.

Figure 4.4 shows the SEM image of grown ZnO nanorods over seeded Si substrate.

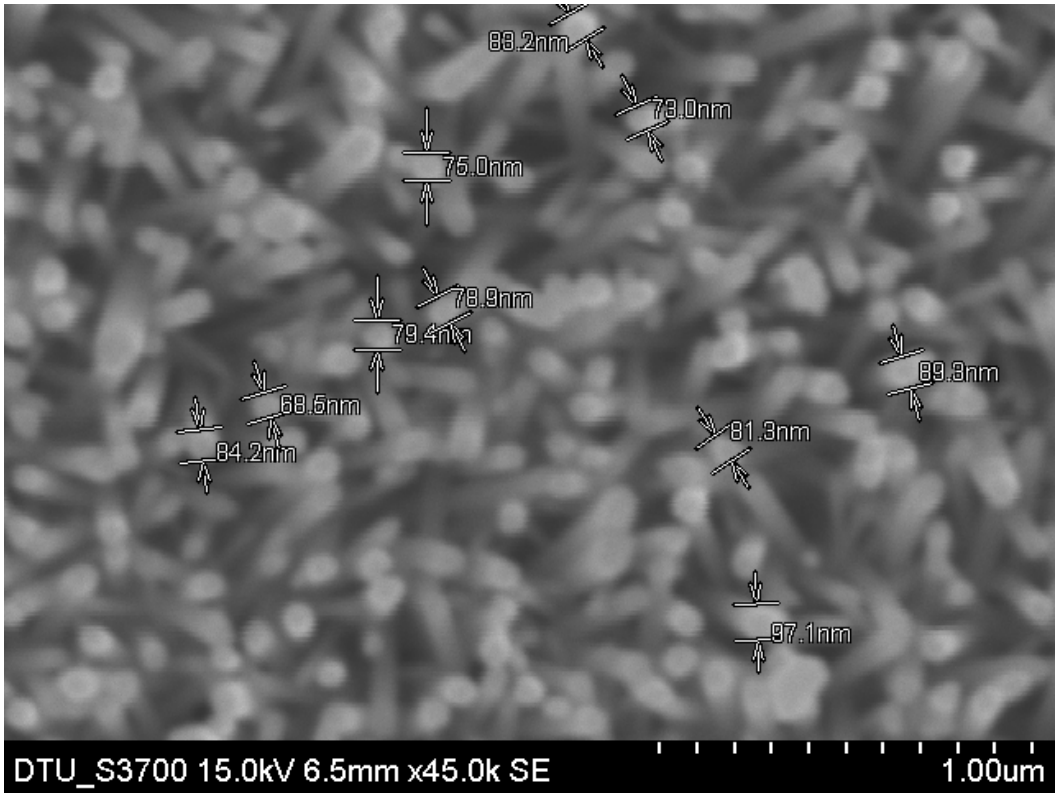

Figure 4.4 SEM image of grown ZnO nanorods on seeded substrate indicating their vertical alignment.

The SEM image of ZnO nanorods grown on seeded substrate (Figure 4.4) indicates that the ZnO nanorods are vertically aligned i.e. c-axis oriented which is only possible when the

orientation of nanorods becomes dominant along (002) plane. It supports the XRD data for the ZnO nanorods with seeded Si substrate (Figure 4.2). The diameter of nanorods is observed within the range of 70 nm to 90 nm. The length of vertically aligned nanorods can be estimated by cross-sectional image which is not recorded here. However, we can assume that the length of vertically aligned ZnO nanorods will be comparable to horizontal one as we kept the same growth time for both kinds of nanorods. In the vertically grown ZnO nanorods sample, overgrowth of ZnO nanorods were also observed as shown in Figure 4.5. Overgrowth can be removed by reducing the growth time or uniform layer deposition of seeds on the substrate.

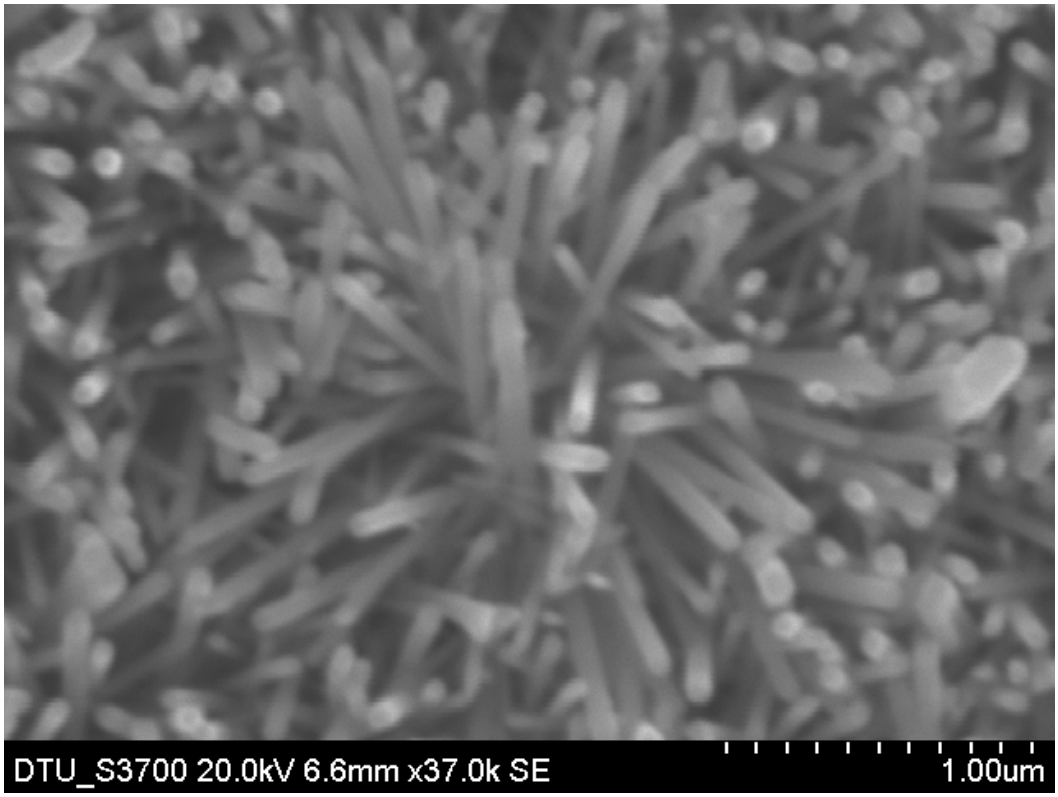

Figure 4.5 SEM image of vertically aligned ZnO nanorods on seeded substrate indicating over growth in some portion of substrate.

4.1.3 Photoluminescence Measurement

To investigate the quality of as grown ZnO nanorods, the photoluminescence (PL) measurement was carried out. Figure 4.6 shows the PL spectra of vertically aligned ZnO nanorods on seeded Si substrate.

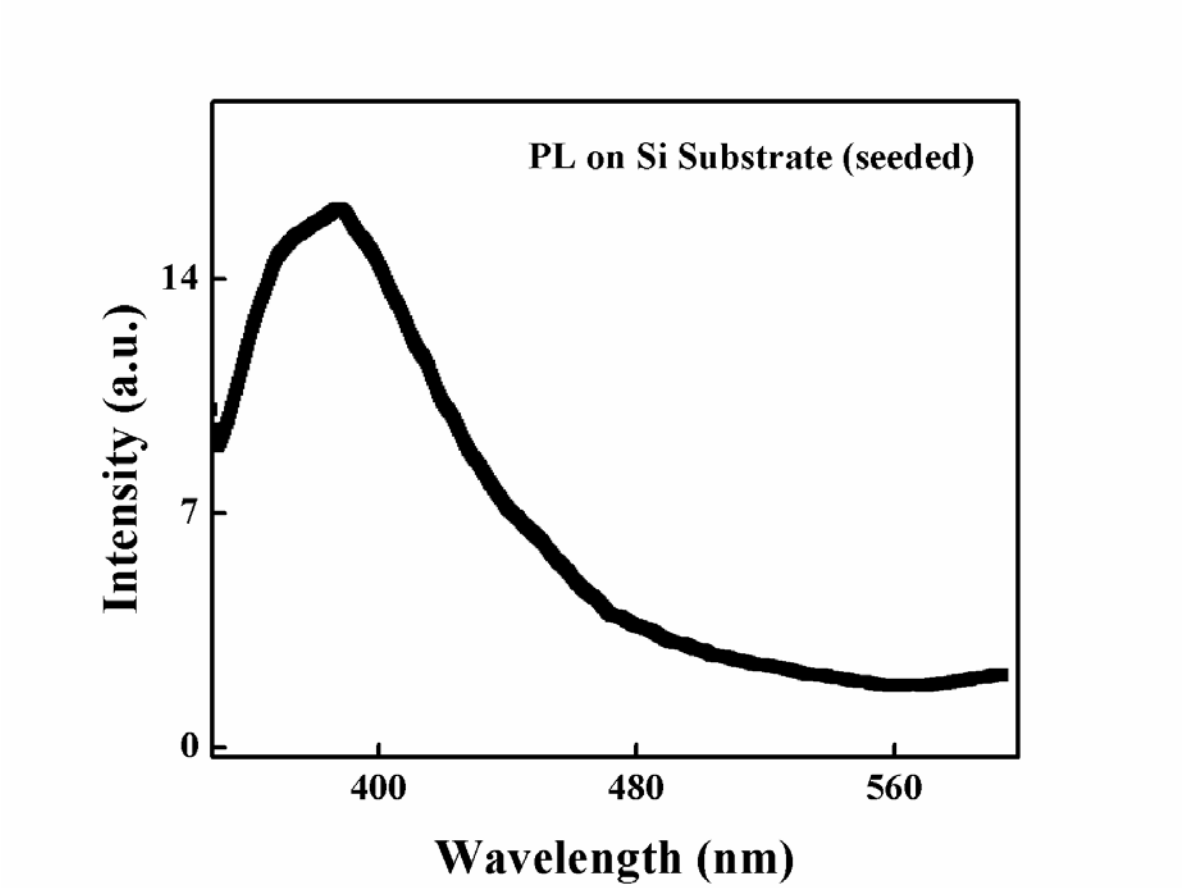

Figure 4.6 PL spectra of vertically aligned ZnO nanorods on seeded Si substrate indicating excitonic peak at 387.8 nm .

The PL spectra of vertically aligned ZnO nanorods (Figure 4.6) exhibit a single peak in UV region at ~ 387.8 nm. It indicates that the as grown ZnO nanorods are of good quality as no defect related broad peak is observed in visible region. The peak at 387.8 nm in UV region

corresponds to 3.20 eV energy and it is comparable to the band gap of ZnO. It reveals that the peak in UV region occur due to end edge emission.

4.1.4 Energy Dispersive x-Ray Spectroscopy

Energy Dispersive x-ray spectroscopy (EDS) measurement was carried out to investigate the elemental analysis of ZnO nanorods. Figure 4.7 shows the EDS spectra of ZnO nanorods.

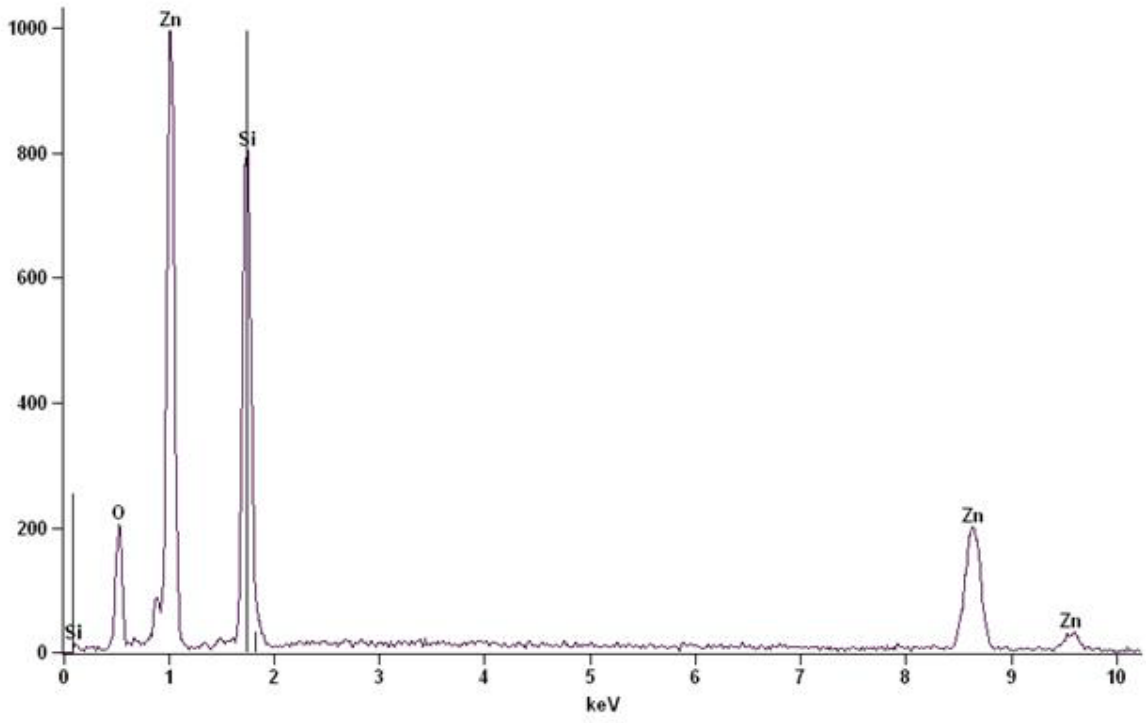

Figure 4.7 EDS spectra of vertically aligned ZnO nanorods on seeded Si substrate.

EDS spectra of vertically aligned ZnO nanorods on seeded Si substrate indicates the presence of Zn, O and Si elements. No other elements corresponding to residue precursors are observed. It indicates that the ZnO nanorods prepared by hydrothermal method consist

of only Zn and O composition indicating their purity. Si elements appears from the substrate.

4.1.5 FeSO4 Doped ZnO Nanorods on Si Substrate

For the application in Li-ion storage devices, flower like morphology on top surface is more desirable as compared to single aligned nanorod. In addition, Fe_2O_3 has been becoming a potential candidate for Li-ion storage devices. Hence, ZnO nanorods grown on Si substrate are doped with $FeSO_4$ to change the morphology as well as to make the ZnO-Fe_2O_3 hybrid structure. Figure 4.8 shows the SEM image of ZnO-Fe_2O_3 flower like hybrid structure of average size ~250 nm.

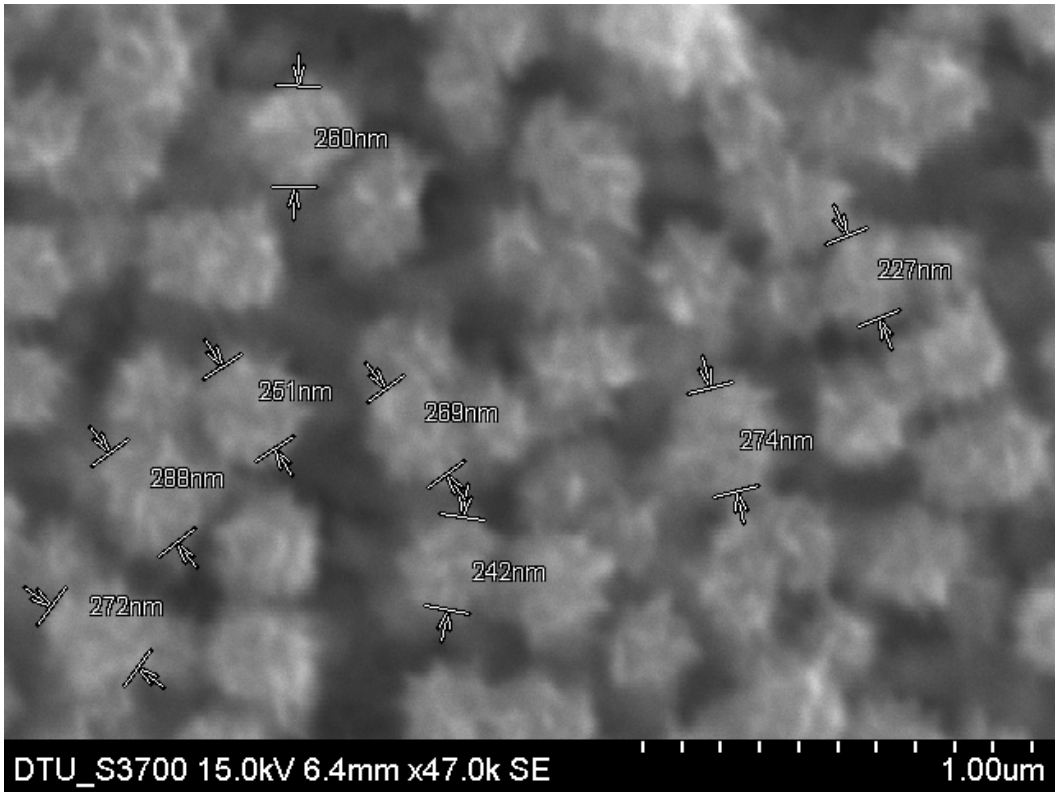

Figure 4.8 SEM image of vertically aligned ZnO nanorods after doping with $FeSO_4$.

4.2 ZnO Nanorods on Cu foil and Doping with Ferrous Sulphate

To explore the potential use of these ZnO nanorods in Li-ion battery application it is desirable to grow the nanorods on metallic substrate which can be compatible to use as current collector in Li-ion storage devices. To fulfill this purpose, ZnO nanorods were grown on Cu foil by employing the similar method like as on Si substrate. Figure 4.9 shows the SEM image of ZnO nanorods grown on Cu foil.

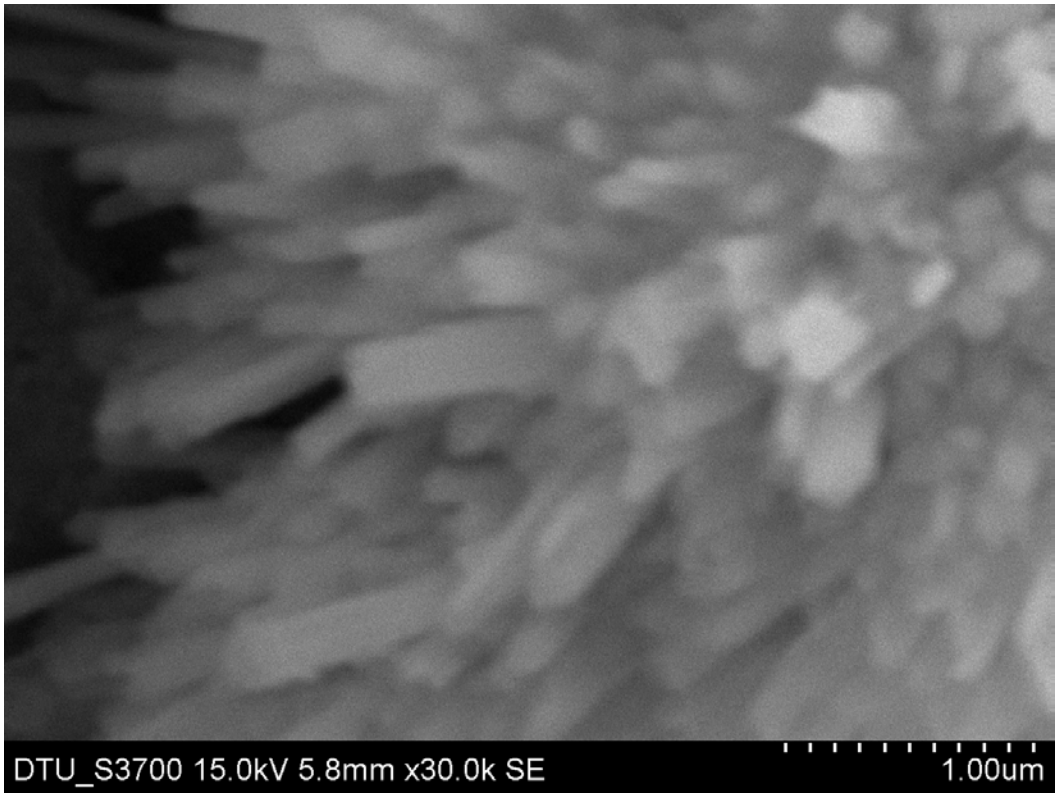

Figure 4.9 SEM image of vertically aligned ZnO nanorods on seeded Cu foil

After growing the ZnO nanorods on Cu foil, nanorods are doped with $FeSO_4$ by employing the same procedure as in case nanorods grown on Si substrate.

The important thing is to observe the morphological behavior of ZnO nanorods on Cu foil after the doping with ferrous sulphate as it plays an crucial role for providing the pores for Li intercalation. The morphological behavior of grown ZnO nanorods on Cu foil with doping of ferrous sulphate has been characterized by scanning SEM image shown in Figure 4.10. Hence, significant changes are noticed in terms of the uniform and dense flower like structures in the SEM image of ZnO nanorods/Cu foil template after doping with ferrous sulphate ($FeSO_4$).

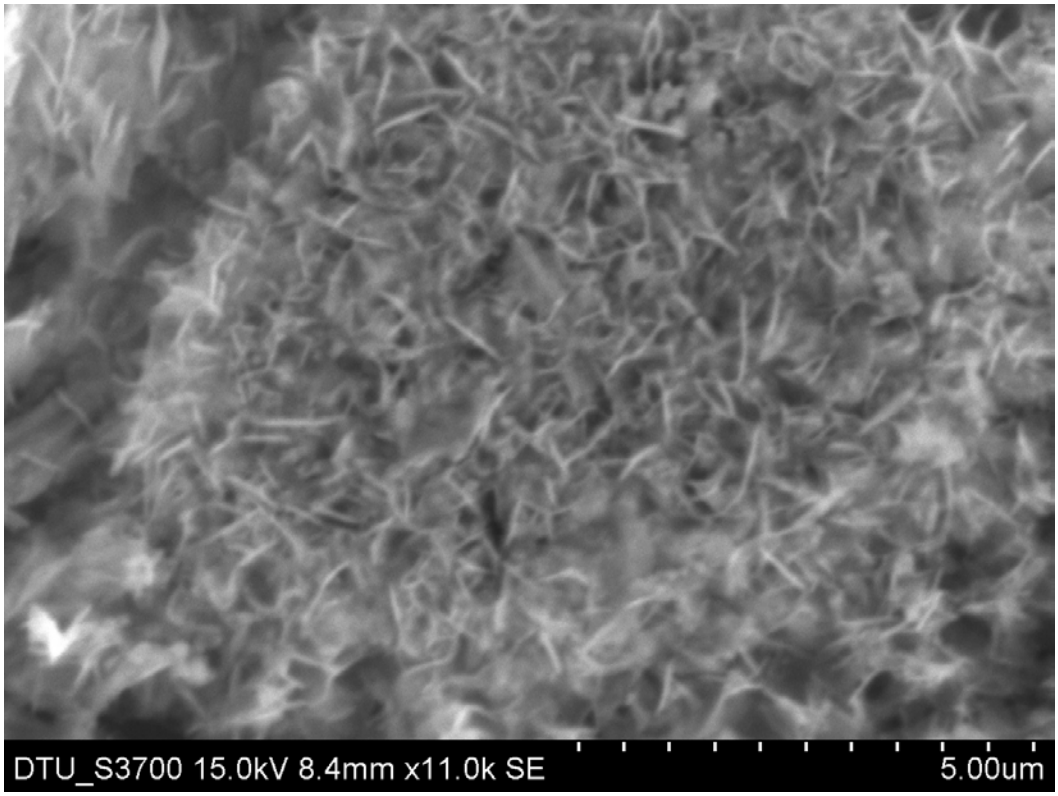

Figure 4.10 SEM image of vertically aligned $FeSO_4$ doped ZnO nanorods on seeded Cu foil

SEM image clearly revels that the vertically aligned ZnO nanorods converted into flower-like structure after doping with $FeSO_4$. The resulted ZnO-Fe_2O_3 hybrid structure can be

useful as an anode electrode in Li-ion battery applications. When ZnO nanorods grown on Cu foil by hydrothermal method are immersed in aqueous solution of $FeSO_4$, top surface of nanorods start to dissolve by H^+ ions produced by the hydrolysis of $FeSO_4$. As a consequence, it accelerated the hydrolysis and plays a crucial role in forming the flower like morphology.

CHAPTER-5

Summary and Future Scope

The growth conditions of ZnO nanorods are optimized using hydrothermal method and the horizontal and vertically aligned ZnO nanorods are successfully grown on seedless and seeded Si substrates, respectively. The purity of phase formation of as grown ZnO nanorods is characterized by XRD and quality of ZnO nanorods is characterized by EDS and PL measurements. These characterizations confirm that the grown ZnO nanorods exhibit pure wurtzite phase of ZnO and of good quality as no features of residual precursor and defects appear. Morphology of as grown ZnO nanorods is studied by SEM which confirms that the orientation of nanorods is horizontal on seedless substrate while on seeded substrate it becomes vertically aligned. Further, vertically aligned ZnO nanorods were grown on Cu foil and dope with $FeSO_4$ to get the formation of ZnO-Fe_2O_3 flower like hybrid structure. Such flower like hybrid structure has a potential use as an anode material in Li-ion battery applications.

The present study sets-up the possible futuristic directions of research based on ZnO nanorods in further improvement in Li-ion storage devices. The performance of Li-ion battery strongly depends on the morphology of the surface of the anode electrode material. The morphology plays a crucial role in deciding the repeated Li-insertion and extraction. Nanoscale surface morphology provides the higher probability to interact and exposes a large surface area for the Li insertion. In addition, periodic morphology in nano form provides higher porosity that also aids for the large amount of Li insertion. In the present

study employed synthesis method provides a way to control and tune the shape, size and structure of ZnO nanorods that can be potentially use in improving the performance of Li-ion battery by further optimization of nanorods.

Moreover, the electrochemical performance of these prepared ZnO based anode materials have to be optimized to the final prediction of potential candidacy as anode material. Electro-chemical analysis may lead to further extension of this work. Hence, there is lot of scope and many issues that need to address related to present work.

REFERENCES

[1] V. Ramadesigan, P.W.C. Northrop, S. De, S. Santhanagopalan, R.D. Braatz and V. Subramanian, J. Electrochem. Soc. 159(3) (2012) R31-R45.

[2] M. Armand and J.M. Tarascon, *Nature*, 451 (2008) 652.

[3] J.M. Tarascon and M. Armand, *Nature*, 414 (2001) 359.

[4] M.S. Whittingham, Science 192 (1976) 1226.

[5] M.S. Whittingham, Chalcogenide Battery, US Patent 4009052.

[6] B.M.L. Rao, R.W. Francis and H.A. Christopher, J. Electrochem. Soc. 124 (1997) 1490.

[7] A.N. Dey, J. Electrochem. Soc. 118 (1971) 1547.

[8] T.R. Jow and C.C. Liang, IBID 129 (1982) 1429.

[9] A.S. Baranskia and W.R. Fawset, J. Electrochem. Soc. 129 (1982) 901.

[10] A. Anani, S. Crouch-Baker and R.A. Huggins, J. Electrochem. Soc. 134 (1987) 3098.

[11] R. Yazami and Ph. Touzain, J. Power Sources 9 (1983) 365.

[12] D.W. Murphy, P.A. Christian, F.J. Disalvo and J.N. Carides, J. Electrochem. Soc. 126 (1979) 497.

[13] M. Lazzari and B. Scrosati, J. Electrochem. Soc. 127 (1980) 773.

[14] T. Nagaura and K. Tozawa, Pro. Batt. Solar Cells 9 (1990) 209.

[15] Yueping (Jane) Yao, Carbon Based Anode Materials for Lithium-Ion Batteries, Master Thesis (2003).

[16] R. Kanno, Y. Takeda, T. Ichikawa, K. Nakamishi and O. Yamamoto, J. Power Sources 26 (1989) 534.

[17] M. Wakihara, Materials Science and Engineering R33 (2001) 109.

[18] H. Zabel, S.A. Solin (Eds.), Graphite Intercalation Compounds I, Springer-Verlag Berlin Heidelberg 1990, Newyork, P6.

[19] X.-M. Liu, Z.D. Huang, S.W. Oh, B. Zhang, P.-C. Ma, M.M.F. Yuen and J.-K. Kim, Composite Science and Technology 72 (2012) 121.

[20] J.R. Dahn, A.K. Sleigh, H. Shi, B.M. Way, W.J. Wegdanz, J.N. Reimers, Q. Gong and U. von Sacken, in G. Pistoia (ed.), Lithium Batteries, Elsevier Science, Amsterdam, 1994.

[21] T. Zheng, J. Electrochem. Soc. 142 (1995) 2581.

[22] T. Enoki, S. Miyajima, M. Sano and H. Inokuchi, J. Mater. Res. 5 (1990) 435.

[23] Y.Q. Song, S.S. Qin, Y.W. Zhang, W.Q. Gao and J.P. Liu, J. Phys. Chem. C 114 (2010) 21158.

[24] S.L. Chou, J.Z. Wang, Z.X. Chen, H.K. Liu and S.X. Dou, Nanotechnology 22 (2011) 265401.

[25] Y. Zhao, J.X. Li, Y.H. Ding and L.H. Guan, Chem. Commun. 47 (2011) 7416.

[26] M.F. Hassan, Z.P. Guo, Z.X. Chen and H.K. Liu, Mater. Res. Bull. 46 (2011) 858.

[27] X.J. Zhu, Y.W. Zhu, S. Murali, M.D. Stollers and R.S. Ruoff, ACS Nano 5 (2011) 3333.

[28] J. Chen and F.Y. Cheng, Acc. Chem. Res. 42 (2009) 713.

[29] L. Qin, Q. Zhu, G. Li, F. Liu and Q. Pan, J. Mater. Chem. 22 (2012) 7544.

[30] P.M. Rao and X.L. Zheng, Nano Lett. 11 (2011) 2390.

[31] X.L. Hu and J.C. Yu, Adv. Funct. Mater. 18 (2008) 880.

[32] W.X. Zhang and S.H. Yang, Acc. Chem. Res. 42 (2009) 1617.

[33] F.Y. Cheng, Z.L. Tao, J. Liang and J. Chen, Chem. Mater. 20 (2008) 667.

[34] U. Ozgur, Y.I. Alivov, C. Liu, A. Teke, M.A. Reshchikov, S. Dogan, V. Avrutin, S.-J. Cho and H. Morkoc, J. Appl. Phys. 98 (2005) 04130.

[35] C. Klingshirn, Chem. Phys. Chem. 8 (2007) 782.

[36] H. Morkoc, “Nitride Semiconductors and Devices”, Springer (2007).

[37] C.W. Bunn, Proc. Phys. Soc. London 47 (1935) 836.

[38] T.C. Damen, S.P.S. Porto and B. Tell, Phys. Rev. 142 (1966) 570.

[39] E. Mollwo, Z. Angew. Phys. 6 (1954) 257.

[40] G. Galli and J.E. Coker, Appl. Phys. Lett. 16 (1970) 439.

[41] C.A. Mead, Phys. Lett. 18 (1965) 218.

[42] I.T. Drapak, Semiconductors 2 (1968) 624.

[43] A.E. Tsurkan, N.D. Fedotova, L.V. Kicherman and P.G. Pas'ko, Semiconductors 6 (1975) 1183.

[44] G.F. Neumark, Phys. Rev. Lett. 62 (1989) 1800.

[45] C.G. Van De Walle, D.B. Laks, G.F. Neumark and S.T. Pantelides, Phys. Rev. B 47 (1993) 9425.

[46] D.B. Laks, C.G. Van De Walle, G.F. Neumark and S.T. Pantelides, Phys. Rev. Lett. 66 (1991) 648.

[47] A. Garcia and J.E. Northrup, Phys. Rev. Lett. 74 (1995) 1131.

[48] C.H. Park, S.B. Zhang and S.-H. Wei, Phys. Rev. B 66 (2002) 073202.

[49] M.L. Cohen, Phys. Scr., T1 (1982) 5.

[50] J. Ihm, A. Zunger and M.L. Cohen, J. Phys. C 12 (1979) 4409.

[51] S.J. Pearton, C.R. Abernathy, M.E. Overberg, G.T. Thaler, D.P. Norton, N. Theodoropoulou, A.F. Hebard, Y.D. Park, F. Ren, J. Kim and L.A. Boatner, J. Appl. Phys. 93 (2003) 1.

[52] C. Liu, F. Yun and H. Morkoc, J. Mater. Sci.: Mater. Elec. 16 (2005) 555.

[53] X.Y. Kong and Z.L. Wang, Nano Lett. 3 (2003) 1625.

[54] W. Wang, B. Zeng, J. Yang, B. Poudel, J. Huang, M.J. Naughton and Z. Ren, Adv. Mater. 18 (2006) 3275.

[55] X. Wang, J. Song and Z.L. Wang, J. Mater. Chem. 17 (2007) 711.

[56] Z.L. Wang, J. Phys.: Condens. Matter 16 (2004) R829.

[57] A.B. Djurisic, A.M.C. Ng and X.Y. Chen, Prog. Quant. Electron. 34 (2010) 191.

[58] S.E. Shaheen, D.S. Ginley and G.E. Jabbour, MRS Bull. 30 (2005) 10.

[59] N. Izyumskaya, V. Avrutin, U. Ozgur, Y.I. Alivov and H. Morkoc, Phys. Stat. Sol. (b) 244 (2007) 1439.

[60] J.B. Lee, H.J. Kim, S.G. Kim, C.S. Hwang, S.-H. Hong, Y.H. Shin and N.H. Lee, Thin Solid Films 435 (2003) 179.

[61] Z.Z. Zhang, D.Z. Shen, Y.M. Lu, J.Y. Zhang, B.H. Li, D.X. Zhao, B. Yao and X.W. Fan, J. Luminescence 122-123 (2007) 202.

[62] V. Craciun, J. Elders, J.G.E. Gardeniers and I.W. Boyd, Appl. Phys. Lett. 65 (1994) 2963.

[63] H.H. Quon and D.P. Malanka, Mat. Res. Bull. 10 (1975) 349.

[64] M. Krunks and E. Mellikov, Thin Solid Films 270 (1995) 33.

[65] M.N. Kamalasanan and S. Chandra, Thin Solid Films 288 (1996) 112.

[66] M. Wei and J.L.M. Driscoll, J. Phys: Confer. Series 26 (2006) 300.

[67] P. Hari, M. Baumer, W.D. Tennyson and L.A. Bumm, J. Non Cryst. Solids 354 (2008) 2843.

[68] M. Kirkham, Z.L. Wang and R.L. Snyder, Nanotechnology 19 (2008) 445708.

[69] X. Kong, X. Sun, X. Li and Y. Li, Mater. Chem. Phys. 82 (2003) 997.

[70] A. Umar, E.-K. Suh and Y.B. Hahn, Solid State Commun. 139 (2006) 447.

[71] S.W. Kim, S. Fujita, H.-K. Park, B. Yang, H.-K. Kim and D.H. Yoon, J. Cryst. Growth 292 (2006) 306.

[72] B. Yang, A. Kumar, H. Zhang, P. Feng, R.S. Katiyar and Z. Wang, J. Phys. D: Appl. Phys. 42 (2009) 045415.

[73] X.-H. Lu, D. Wang, G.-R. Li, C.-Y. Su, D.-B. Kuang and Y.X. Tong, J. Phys Chem. C 113 (2009) 13574.

[74] H.V. Rul, D. Mondelaers, M.K.V. Bael and J. Mullens, J. Sol-Gel Sci. Technol. 39 (2006) 41.

[75] H. Zhang, D. Yang, Y. Ji, X. Ma, J. Xu and D. Que, J. Phys. Chem. B 108 (2004) 3955.

[76] B.K. Sharma, N. Khare and M. Kumar, J. Nanosci. Nanotechnol. 10(12) (2010) 8424.